doi.org/10.1002/cbdv.202300944 Research Article CHEMISTRY & BIODIVERSITY

www.cb.wiley.com

Synthesis of Imidazole-2,3-dihydrothiazole Compounds as VEGFR-2 Inhibitors and Their Support with *in Silico* Studies

Derya Osmaniye,*[a, b] Nurnehir Baltacı Bozkurt,[c] Berkant Kurban,[d] Gamze Benli Yardımcı,[c] Yusuf Ozkay,[a, b] and Zafer Asım Kaplancıklı[a]

In this study, 12 novel 2-((1-(4-(1*H*-imidazol-1-yl)phenyl)ethylidene)hydrazineylidene)-3-ethyl-4-(substitute-phenyl)-2,3-dihydrothiazole derivatives were obtained. Among these compounds, 2-((1-(4-(1*H*-imidazol-1-yl)phenyl)ethylidene)hydrazineylidene)-4-([1,1′-biphenyl]-4-yl)-3-ethyl-2,3-dihydrothiazole (**4h**) was chosen as the most active derivative in the series. According to the MTT results, compounds **4h** and **4k** showed activity with $IC_{50} = 4.566 \pm 0.246$ μM and $IC_{50} = 4.537 \pm 0.463$ μM, respectively. Unlike other derivatives, compound **4h** carries a phenyl ring in the 4th position of the phenyl ring. This bulky group allowed the compound to settle in the enzyme active site. Dynamic studies show that the stability of the compound does not change over 40 ns. RMSD, RMSF and Rg parameters all remained within acceptable limits. The uninterrupted aromatic hydrogen bonding of the enzyme active site with the important amino acids Cys919, Glu885 and Asp1046 proves the inhibitory potential of compound **4h** on the VEGFR-2 enzyme. It is thought that more active compounds will be reached with the derivatives to be synthesized starting from compound **4h**.

Introduction

Cancer, one of the deadliest diseases that terribly endanger human life, causes 13% of annual global deaths.[1] According to the World Health Organization (WHO), cancer-related deaths were reported as ten million in 2020.[2,3] Receptor tyrosine kinases (RTKs) are prominent targets for cancer therapy. They are a primary target because of the important roles they play in cancer pathophysiology.[4]

Targeted drug therapy uses drugs that specifically target proteins that support the growth, spread, and survival of cancer cells. These targets include macromolecules such as epidermal growth factor receptor (EGFR), human epidermal growth factor receptor Type 2 (HER2) and vascular endothelial growth factor (VEGF).[5]

Vascular endothelial growth factor receptor-2 (VEGFR-2) is a trans-membrane tyrosine kinase receptor. VEGFR-2 inhibitors have an effective and critical role in cancer treatment. A new agent that affects the inhibition and downregulation of the VEGFR-2 signaling chain may be the first step in the discovery of a new chemotherapeutic.[6] VEGFR-2 inhibitors, which effectively prolong progression-free survival and overall survival of tumor patients, have some bad properties. One of these side effects is the *in vivo* accumulation of inactivated VEGFR-2 protein. The degree of this accumulation varies according to the use of multiple or long-term drug therapy.[7] Following the initial treatment with approved VEGFR-2 inhibitors, secondary resistance demonstrates the need to develop new therapeutic alternatives.[8]

Figure 1 summarizes the pharmacophoric properties of sorafenib, a known VEGFR-2 inhibitor. It is possible to mention 4 pharmacophore parts for VEGFR-2 inhibitors. While developing a new inhibitor candidate, taking these structures as a basis will enable to reach effective compounds. The initial pharmacophore for VEGFR-2 inhibitors requires the presence of a hydrophobic head. The second part should contain a hydrogen bond donor and acceptor, which interact with Glu885 and Asp1046 to occupy the DFG motif site. The third pharmacophoric moiety is a flat heteroaromatic ring occupying the adenine binding pocket, which is considered a dividing moiety for VEGFR-2 inhibitors. Finally, the fourth pharmacophoric feature is the hinge region of VEGFR-2 inhibitors.[9]

The thiazole ring is very useful in terms of biological activity. There is a lot of literature information showing its anticancer and antifungal activity.[10–17] In addition to this information, there is also a study using the thiazole ring as a VEGFR-2 inhibitor.[18] When docking studies are examined, the interaction of the thiazole ring with Asp1046, which is an important amino

[a] *Dr. D. Osmaniye, Prof. Dr. Y. Ozkay, Prof. Dr. Z. A. Kaplancıklı*
Department of Pharmaceutical Chemistry,
Faculty of Pharmacy,
Anadolu University,
26470 Eskişehir, Turkey
E-mail: dosmaniye@anadolu.edu.tr

[b] *Dr. D. Osmaniye, Prof. Dr. Y. Ozkay*
Central Analysis Laboratory,
Faculty of Pharmacy,
Anadolu University,
26470 Eskişehir, Turkey

[c] *Dr. N. B. Bozkurt, G. B. Yardımcı*
Department of Pharmaceutical Microbiology,
Faculty of Pharmacy,
Afyonkarahisar Health Sciences University,
03030 Afyonkarahisar, Turkey

[d] *B. Kurban*
Department of Pharmaceutical Chemistry,
Faculty of Pharmacy,
Afyonkarahisar Health Sciences University,
03030 Afyonkarahisar, Turkey

Supporting information for this article is available on the WWW under https://doi.org/10.1002/cbdv.202300944

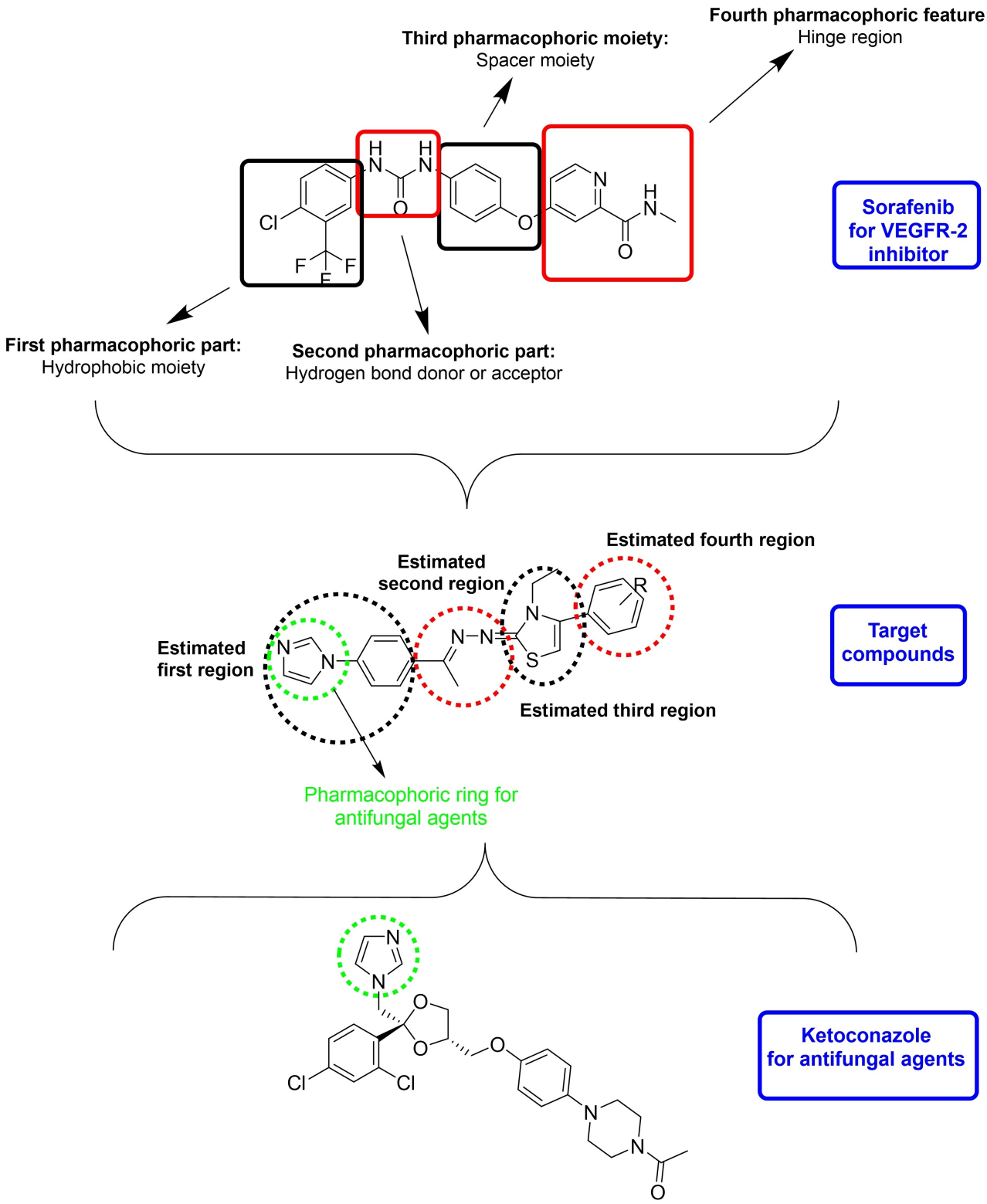

Figure 1. Pharmacophoric properties of Sorafenib and design strategy of compounds **4a**–**4l**.

acid for the enzyme, shows the potential of the ring to inhibit VEGFR-2.

The development of new VEGFR-2 inhibitors will both prevent resistance to existing drugs and provide access to more effective derivatives. In this study designed for this purpose, attention was paid to the pharmacophoric parts of VEGFR-2 inhibitors (Figure 1). At the same time, it is aimed to create a synergistic effect by using structures with known anticancer activity (thiazole, imidazole). Imidazole and its associated phenyl are also considered as the hydrophobic head to occupy

the hydrophobic site in the VEGFR-2 active site. An ethylidenehydrazineylidene bridge connects this hydrophobic head to the thiazole ring. The substituted phenyl ring attached to the thiazole ring is designed to be placed in the hinge region.

It is very important for patient use that a drug candidate shows both anticancer and antifungal activity. Because cancer patients become immune to most fungal infections during treatment. For this reason, when developing a VEGFR-2 inhibitor, it was thought that if the heteroatom-containing ring that would be preferred as a pharmacophore group was imidazole (pharmacophore group in terms of antifungal drugs), the compounds could also exhibit antifungal properties. In addition to the imidazole ring being in the structure of antifungal drugs, there are many reports in the literature showing the antifungal activity of this ring system.[19–24]

In the light of all this information, new imidazole-2,3-dihydrothiazole compounds were synthesized to develop novel VEGFR-2 inhibitor.

Table 1. Anticancer activity of obtained compounds (**4a**–**4l**)

Compound	IC_{50} (μM)		
	MCF-7	HepG2	NIH3T3
4a	14.461 ± 0.908	11.899 ± 0.458	38.048 ± 1.141
4b	21.176 ± 1.452	23.199 ± 0.985	50.019 ± 2.297
4c	87.488 ± 4.258	> 100	> 100
4d	> 100	> 100	25.844 ± 1.017
4e	24.820 ± 0.471	32.250 ± 1.128	29.709 ± 0.289
4f	12.122 ± 0.689	24.126 ± 1.036	11.808 ± 0.319
4g	11.785 ± 0.149	19.979 ± 0.845	3.671 ± 0.154
4h	14.004 ± 0.294	4.566 ± 0.246	13.239 ± 0.287
4i	43.746 ± 1.185	**43.928 ± 1.258**	17.300 ± 0.524
4j	13.731 ± 0.942	12.357 ± 0.781	12.981 ± 0.193
4k	32.353 ± 0.497	**4.537 ± 0.463**	12.341 ± 0.208
4 l	34.711 ± 0.399	19.031 ± 0.869	25.288 ± 0.497
Sorafenib	7.011 ± 0.139	8.536 ± 0.368	> 100

[n] The test results were expressed as means of quartet assays ± SD

Results and Discussion

Chemistry

The compounds **4a**–**4l** were gained using four step synthesis reaction. This reaction pathway was presented in Scheme 1. Firstly, **compound 1** was obtained using microwave reactor. Secondly, **compound 2** was obtained with reaction between **compound 1** and hydrazine hydrate. Thirdly, thiosemicarbazone derivative (**3**) was synthesized by means of the reaction between **compound 1** and **compound 2**. Finally, the target compounds (**4a**–**4l**) were obtained using ring closure reaction. The structures of the obtained compounds were evaluated by spectroscopic methods, namely ^{1}H-NMR, ^{13}C-NMR, and HR-MS (**Supplementary Data**).

Cytotoxicity Test

The 24-h MTT procedure was applied for the activity tests. 2 cancer cell lines and 1 healthy cell lines were used in cytotoxicity studies. While MCF-7 (ATCC HTB-22) and HepG2 (ATCC HB-8065) are used as cancer cells; NIH3T3 (ATCC CRL-1658) was used as healthy cell. The obtained activity results are promising (Table 1). Most of the compounds showed activity with an $IC_{50} < 100$ μM. One of the remarkable points is that compound **4g** showed cytotoxicity with $IC_{50} = 3.671 \pm 0.154$ μM against NIH3T3 cell lines. The same compound (**4g**) showed activity against MCF-7 and HepG2 cell lines, with $IC_{50} = 11.785 \pm 0.149$ μM and $IC_{50} = 19.979 \pm 0.845$ μM, respectively. This suggests that compound **4g** is cytotoxic. Looking at the structure of the compound, it is seen that it contains bromine substituent. A similar occurrence applies to compound **4d**. Compound **4d** showed activity against MCF-7 and HepG2 cells with $IC_{50} > 100$ μM; it showed cytotoxicity against NIH3T3 cell lines with $IC_{50} = 25.844 \pm 1.017$ μM. Compound **4d** carries the nitro substituent. It can be thought that these two substituents (Br and NO_2) increase toxicity.

On the other hand, compounds **4h** and **4k** showed activity with $IC_{50} = 4.566 \pm 0.246$ μM and $IC_{50} = 4.537 \pm 0.463$ against HepG2 cell lines, respectively. The selectivity indexes of these compounds were calculated as 2.90 and 2.72, respectively. Compound **4h** carries the phenyl substituent in the 4th position; compound **4k** carries chlorine substituent at 2nd and 4th positions. The inclusion of a bulky group at the 4th position appears to increase activity for the HepG2 cell lines (such as compound **4h**).

When all compounds containing chlorine substituent are examined (**4f**, **4k** and **4 l**); the chlorine substituent brought alone to the 4th position (**4f**) exhibited cytotoxic activity. Compound **4f** showed cytotoxicity with $IC_{50} = 11.808 \pm 0.319$ μM against NIH3T3 cell lines. A similar situation is seen in all compounds (**4e**–**4g**) containing halogen in the 4th position. In addition to the halogen in the 4th position, the cytotoxicity was decreased with similar halogen substituents brought to the second position (compounds **4j** and **4k**). In fact, the activity increased bearing the 2,4-dichloro substituent for the compound **4k**. When the 3,4-dichloro-bearing compound (**4 l**) is examined, it is seen that the cytotoxicity decreases and the activity increases. But the increase in activity is not as promising as composite **4k**.

Antifungal Activity

Determination of the minimum inhibitory concentration (MIC)

The anticandidal activities of the obtained compounds were evaluated using *C. albicans*, *C. glabrata*, *C. tropicalis* and *C. krusei* strains. The obtained data are presented in Table 2. The obtained data show that compounds (**4a**–**4l**) exhibit activity

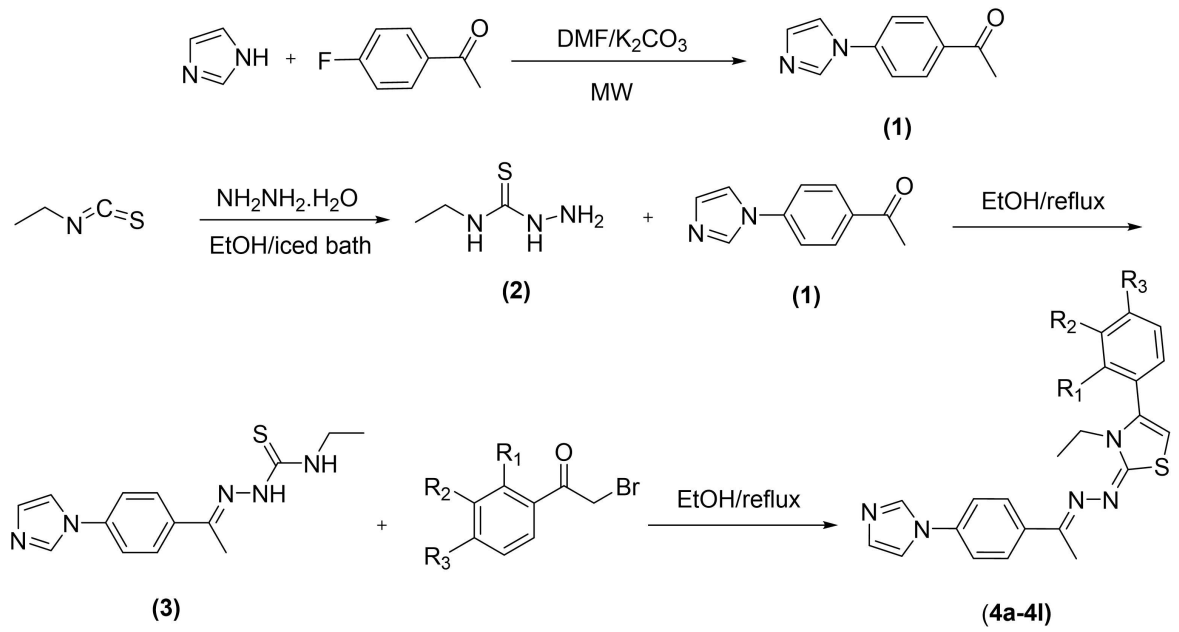

Comp.	R_1	R_2	R_3
4a	-H	-H	$-CH_3$
4b	-H	-H	$-OCH_3$
4c	-H	-H	-CN
4d	-H	-H	$-NO_2$
4e	-H	-H	-F
4f	-H	-H	-Cl
4g	-H	-H	-Br
4h	-H	-H	-phenyl
4i	$-CH_3$	-H	$-CH_3$
4j	-F	-H	-F
4k	-Cl	-H	-Cl
4l	-H	-Cl	-Cl

Scheme 1. The synthetic route for target compounds (**4a**–**4l**).

profiles between MIC_{90} = 32-128 μg/mL. Compound **4h** showed activity against *C. albicans*, *C. glabrata* and *C. tropicalis* with a value of MIC_{90} = 64 μg/mL and with a value of MIC_{90} = 128 μg/mL against *C. krusei*. Compound **4k** showed activity against *C. glabrata*, *C. tropicalis* and *C. krusei* with a value of MIC_{90} = 128 μg/mL and with a value of MIC_{90} = 64 μg/mL against *C. albicans*.

Antibiofilm activity against Candida species

Structured microbial populations that are connected to a surface and enclosed in an extracellular matrix that they have formed themselves are known as biofilms. A crucial aspect of infection is that Candida spp. can attach to and create biofilms on biological surfaces and implanted medical devices. Compared to planktonic cells, microbial biofilms are considerably more resistant to several antimicrobial treatments because they serve as protective reservoirs for the bacteria.[25] Surgical interventions in patients receiving chemotherapy or cases where drug intake is provided by port can be considered as

Table 2. Antifungal activity of obtained compounds (**4a**–**4l**).

Compound	*C. albicans* ATCC 10231	*C. glabrata* ATCC 2951	*C. tropicalis* ATCC 750	*C. krusei* ATCC 34135
4a	64	64	64	64
4b	64	64	64	128
4c	64	64	64	64
4d	64	64	64	128
4e	64	64	64	128
4f	32	64	64	128
4g	32	64	128	64
4h	64	64	64	128
4i	32	64	64	32
4j	64	128	64	128
4k	64	128	128	128
4 l	64	128	128	128
Fluconazole	0,5	2	4	16

[n] The test results were expressed as means of triplicate assays.

open to biofilm infection. For this purpose, it would be useful for a compound with anticancer activity to show antibiofilm activity at the same time. For each compound, MIC/2, MIC and 2xMIC concentrations were studied. Obtained results are presented in Table 3.

VEGFR-2 Inhibition Assay

The VEGFR-2 Kinase Assay Kit (Available from[26]) was used for the VEGFR-2 inhibition. The experiment was performed *in vitro* according to the kit procedure. Serial 11 dilutions of compounds **4h** and **4k** were prepared at concentrations of 1000 μM-0.01 μM. The IC_{50} value for compounds **4h** and **4k** was calculated using the kit procedure. According to the obtained results (Table 4), the compound **4h** shows inhibitory activity on VEGFR-2 enzyme with the value of $IC_{50} = 0.066 \pm 0.002$ μM. However, the compound **4k** shows inhibitory activity on VEGFR-2 enzyme with the value of $IC_{50} > 10$ μM.

Table 4. VEGFR-2 Inhibition of compounds **4h**, **4k** and sorafenib.

Compound	IC_{50} for VEGFR-2 Inhibition (μM)
4h	0.066 ± 0.002
4k	> 10
Sorafenib	0.044 ± 0.002

Molecular Docking Studies

PDB ID:4ASE crystal was used to examine the localization of the compounds in the VEGFR-2 enzyme active site. Firstly, the location of both compounds (**4h** and **4k**) and the reference drug sorafenib were examined (Figure 2) in the active region of VEGFR-2 enzyme. Sorafenib was colored blue, compound **4h** colored pink, and compound **4k** colored orange.

When this image is examined, it is clearly understood why compound **4k** does not show activity on the VEGFR-2 enzyme. Compound **4h** and sorafenib overlap exactly. In fact, Figure 3 can be examined for a clearer understanding of this image.

However, as can be seen in Figure 2, a large part of compound **4k** does not overlap with other molecules. Com-

Table 3. Biofilm percent inhibitions results of synthesized compounds (**4a**–**4l**) and standard drug (fluconazole).

Compound	*C. albicans* ATCC 10231			*C. glabrata* ATCC 2951			*C. tropicalis* ATCC 750			*C. krusei* ATCC 34135		
	2×MIC	MIC	½×MIC	2×MIC	MIC	½×MIC	2×MIC	MIC	½×MIC	2×MIC	MIC	½×MIC
4a	40	37	29	38	34	31	68	65	65	68	67	60
4b	60	52	54	37	38	38	68	67	66	70	66	64
4c	74	74	73	40	32	31	67	64	64	65	65	62
4d	73	69	66	34	34	31	68	66	64	70	65	62
4e	42	34	14	33	38	23	68	66	66	64	62	61
4f	51	40	33	38	38	31	69	69	68	65	61	61
4g	50	38	28	38	31	33	69	69	67	65	62	54
4h	61	62	58	71	70	69	71	70	69	72	68	53
4i	67	62	54	71	70	67	71	71	67	68	68	52
4j	62	64	57	71	70	66	71	70	66	73	68	52
4k	66	63	46	70	72	68	71	71	63	74	71	59
4 l	68	65	52	76	72	70	76	72	68	78	78	59
Fluconazole	67	64	62	84	80	79	77	76	70	78	76	60

[n] The test results were expressed as means of triplicate assays.

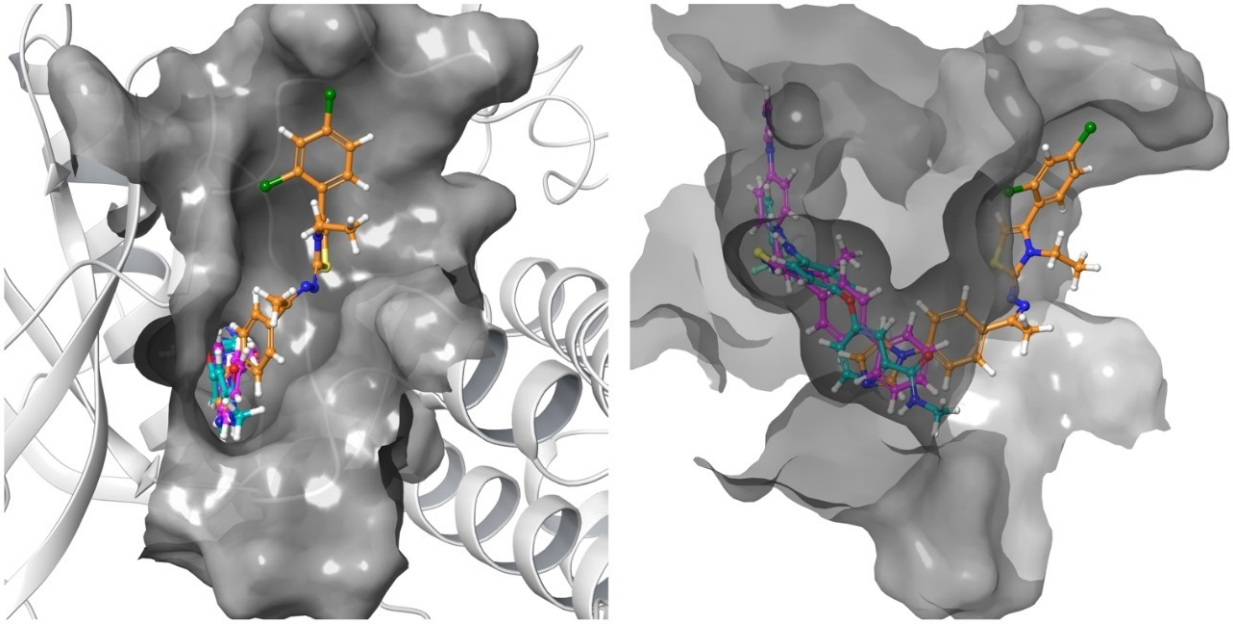

Figure 2. Localization of compounds **4h**, **4k** and sorafenib at the enzyme active site of VEGFR-2 (PDB ID:4ASE). **4h** is colored pink, **4k** is orange and sorafenib is colored blue.

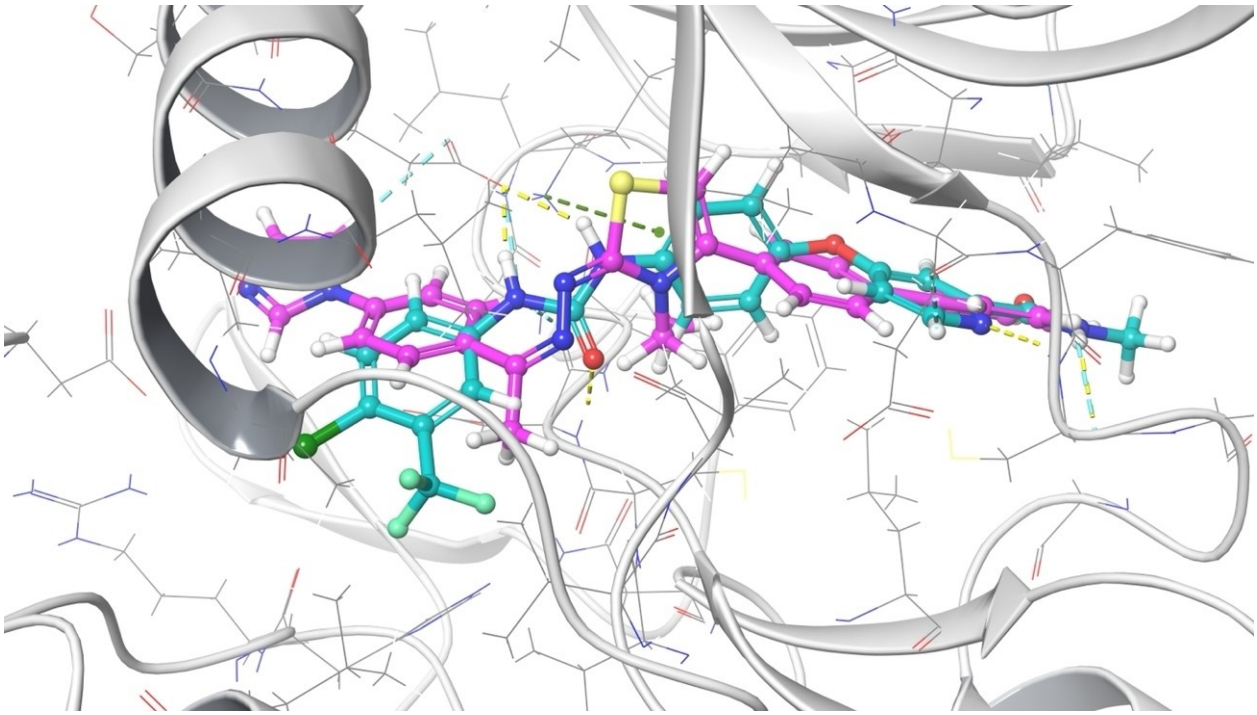

Figure 3. Overlapping exposure of compound **4h** and sorafenib at the enzyme active site of VEGFR-2 (PDB ID:4ASE).

pound **4k** showed a localization outside the active site of the enzyme.

The interactions of compound **4h** are presented in Figure 4. It forms an aromatic hydrogen bond between the monosubstituted phenyl ring and Cys919. The 4,5-dihydrothiazole ring has pi-pi interaction with the amino group of Lys868. The phenyl group attached to the imidazole ring formed aromatic hydrogen bonds with the carbonyl of Asp1046 and the hydroxy group of Glu885. Finally, a hydrogen bond was noted between the imidazole ring and the carbonyl group of Glu885.

Molecular Dynamic Simulation (MDS) studies

Molecular dynamics studies carried out within the scope of this study were carried out on the **4h**–4ASE complex. In the study,

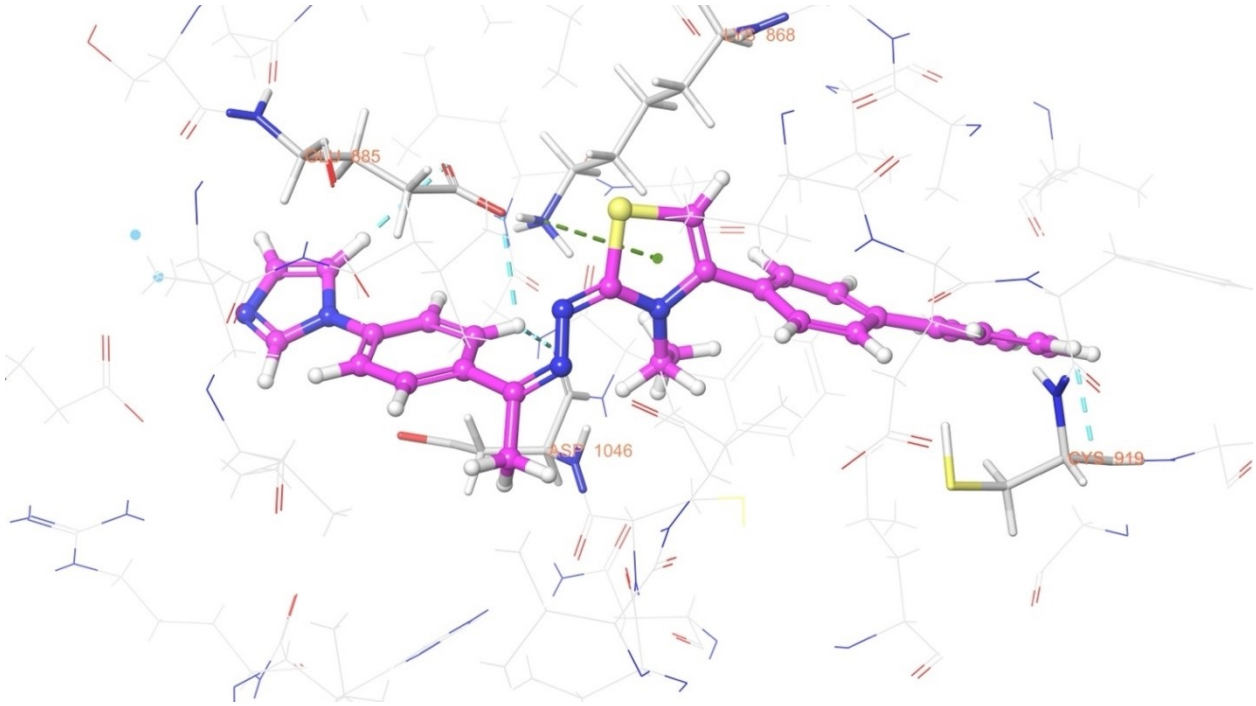

Figure 4. Three-dimensional visualization of the interaction of compound **4h** with the VEGFR-2 (PDB ID:4ASE) enzyme active site.

which was carried out for 40 ns, POPC was used as the membrane model and the temperature was set as 300 K. Root mean square deviation of atomic coordinates (RMSD) is the most frequently used value to measure both macromolecular structures and dynamic differences in optimal rigid body superposition of two structures.[27] The RMSD as a function of the simulation time of **4h**–4ASE complex were analyzed during 40 ns as shown in Figure 5A, 5 C. Figure 5A also showed the RMSD between the starting conformations and the ones during the MD simulation are less than 2 Å. As can be seen, the RMSD value reveals the stability of the complex. In addition, it is seen that the slight fluctuations that occur completely disappear after 25 ns.

It is known that individual amino acids are another factor that plays a role in MD simulation. These amino acids are especially important in terms of ensuring the stability of the complex. The RMSF parameter provides information on fluctuation and conformational changes of individual amino acids within the simulation period (Figure 5B). If the atoms in the active site and the main chain are slightly shifted, this means that the conformational change is small; this means that the proposed compound binds tightly to the active site of the VEGFR-2 protein.[28–30]

As per RMSF plot (Figure 5B), compound **4h** contacted 24 amino acids of VEGFR-2 protein, namely, Asp814 (1.36 Å), Lys838 (0.92 Å), Leu840 (0.77 Å), Val848 (0.52 Å), Ala866 (0.46 Å), Lys868 (0.51 Å), Ser884 (0.78 Å), Glu885 (0.68 Å), Ile888 (0.67 Å), Leu889 (0.60 Å), Ile892 (0.81 Å), Val898 (0.55 Å), Val899 (0.61 Å), Glu917 (0.66 Å), Phe918 (0.61 Å), Cys919 (0.57 Å), Ile1025 (0.55 Å), His1026 (0.50 Å), Arg1027 (0.53 Å), Leu1035 (0.47 Å), Cys1045 (0.48 Å), Asp1046 (0.51 Å), Phe1047 (0.52 Å), Leu1049 (0.74 Å).

The radius of rotation (Rg), defined by the mean square root distance between the center of gravity and all atoms in a molecule, which can be determined by the compactness of the macromolecule structure, represents the structure compactness, especially in protein analysis[31] The Rg value of the **4h**–4ASE complex is presented in Figure 5D. When the analysis obtained was examined, it generally varied between 5.8 Å and 6.2 Å. Around 20 ns, a fluctuation of only 0.2 Å (5.8 Å −6.0 Å) occurred. This once again demonstrates the stability of the complex.

By watching the MD Simulation video, aromatic hydrogen bonds were determined for 40 ns seconds. Compound **4h** formed aromatic hydrogen bonds with Glu917, Cys919, Glu885, Asp1046, Val867, Asp814 and Asn923. When Figure 6 is examined, the interactions of compound **4h** with VEGFR-2 enzyme are seen. **6 A** depicts amino acid interactions over time, **6B** illustrates amino acid fractions with interaction, and finally **6 C** depicts amino acids with 7% or more interaction.

Examining Figure 6A, it is seen that compound **4h** interacts uninterruptedly with Leu840, Ala866, Leu889, Val916, Phe918, Leu1035 and Phe1047. Apart from these amino acids, high levels of interaction were also observed with Val848, Lys868 and Ile888.

Compound **4h** at the VEGFR-2 enzyme active site based on the interaction fractions presented in Figure 6B. This amino acide fractions listed as Asp814, Lys838, Leu840, Val848, Ala866, Lys868, Ser884, Glu885, Ile888, Leu889, Ile892, Val898, Val899, Val916, Phe918, Cys102519, Ile Interacted with His1026, Arg1027, Leu1035, Cys1045, Asp1046, Phe1047, Leu1049.

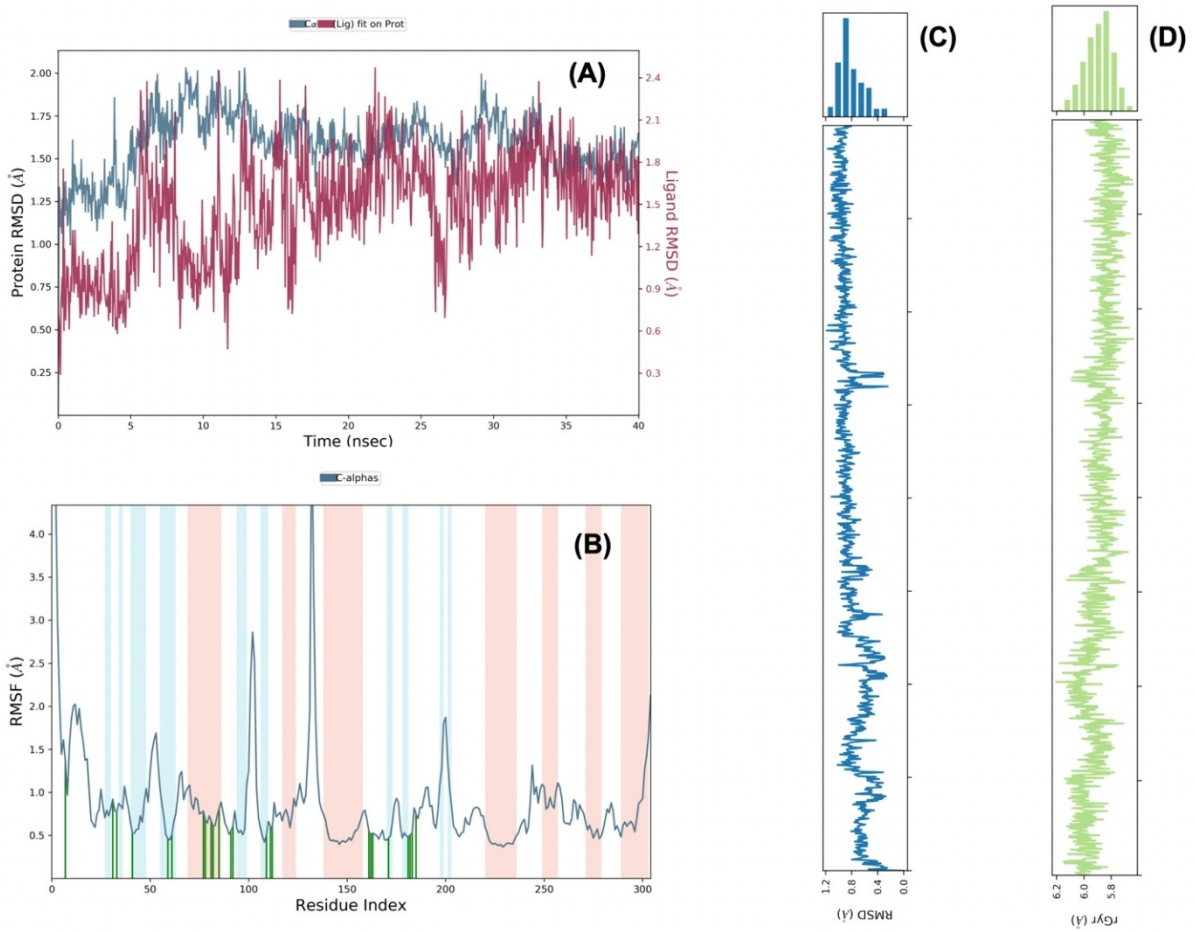

Figure 5. The stability results of compound **4h**. A and C presented of RMSD analysis; B presented RMSF analysis and D presented Rg analysis.

The contribution of each of these amino acids to stability is indisputable. However, the lack of interaction with amino acids (Asp1046 and Glu885) in the DFG motif, which is considered important for inhibitory activity, draws attention. When the video is watched, it is seen that compound 4h makes continuous aromatic hydrogen bonds with these amino acids. Similarly, it is seen that it makes continuous aromatic hydrogen bonds with Cys919, which is considered one of the important amino acids of the hinge region. These interactions are also the results obtained by in vitro experiments.

Conclusions

Oral kinase inhibitors have been used frequently in cancer chemotherapy in recent years. When the structure of VEGFR inhibitors is examined, it is seen that it consists of 4 pharmacophoric parts. In the light of this information, within the scope of this study, new 2-((1-(4-(1*H*-imidazol-1-yl)phenyl)ethylidene)hydrazineylidene)-3-ethyl-4-(substitute-phenyl)-2,3-dihydrothiazole derivatives were synthesized. Structure determinations of the synthesized derivatives were made using spectroscopic methods. Firstly, the resulting compounds (**4a**–**4l**) were subjected to the 24-h MTT test against MCF7, HepG2 and NIH3T3 cells. According to the MTT test results, compound **4h** showed activity with $IC_{50} = 4.566 \pm 0.246$ μM and compound **4k** with $IC_{50} = 4.537 \pm 0.463$ μM against HepG2 cell lines. The antifungal activities and biofilm inhibition percentages of all compounds against infection problems that may develop in patients receiving chemotherapy were investigated. Accordingly, the compound **4h** showed biofilm inhibition against *C. tropicalis* with rates of 71%, 70%, 69% (2MIC, MIC, MIC/2). This ratio is like fluconazole (reference drug). Compounds **4h** and **4k** which are active in the MTT test were tested for inhibition of VEGFR-2 enzymes using *in vitro* kit procedure. Compound **4h** displayed VEGFR-2 inhibition with $IC_{50} = 0.066 \pm 0.002$ μM value; compound **4k** did not show enzyme inhibition with an $IC_{50} > 10$ μM. Molecular docking studies were performed with two compounds (**4k** and **4h**) and sorafenib to understand the dramatic difference for VEGFR-2 inhibition. It was noted that while compound **4k** and sorafenib were located on the enzyme active site, most of compound **4h** was located outside the enzyme active site. This, activity made the difference to be understood. Molecular dynamics studies were performed with using **4h**–4ASE complex and both stability (RMSD, RMSF, Rg)

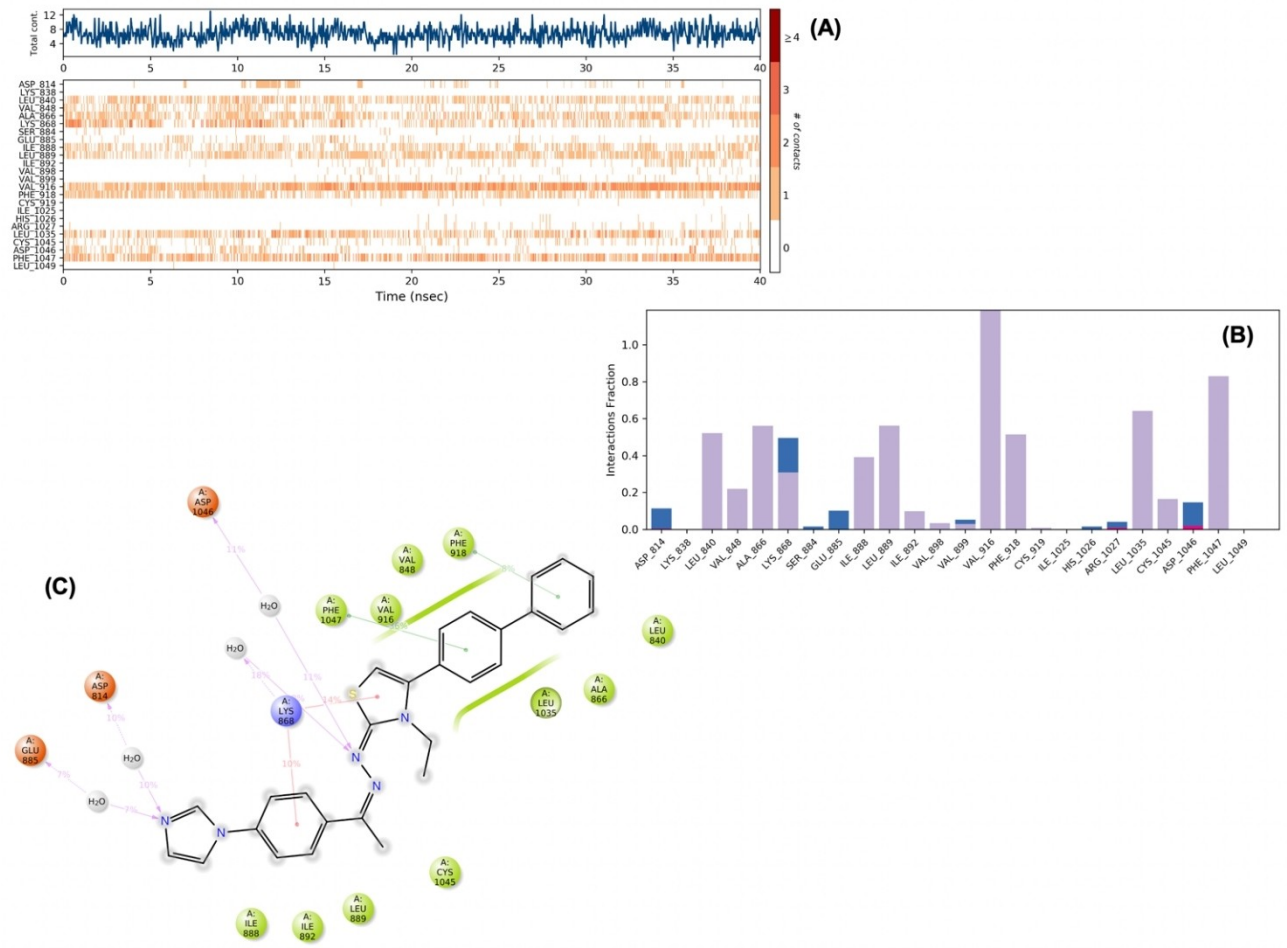

Figure 6. Interaction results of compound **4h** for 40 ns MD simulations.

and interaction potentials of the complex were analyzed and presented.

Experimental Section

Chemistry

General

All reagents were purchased from commercial suppliers and were used without further purification. Melting points (M.p.) were determined on the Mettler Toledo-MP90 Melting Point System and were uncorrected. ^{1}H-NMR (nuclear magnetic resonance) Bruker DPX 300 FT-NMR spectrometer; ^{13}C-NMR, Bruker DPX 75 MHz spectrometer (Bruker Bioscience, Billerica, MA, USA). Mass spectra were recorded on a LCMS-IT-TOF (Shimadzu, Kyoto, Japan) using ESI.

Synthesis of 1-(4-(1H-imidazol-1-yl)phenyl)ethan-1-one (1)

Imidazole (0.07 mol) and 4-fluoroacetophenone (0.07 mol) were dissolved in DMF (10 mL). K_2CO_3 was used as catalyzer. The reaction mixture was put in microwave reactor. And the reaction conditions were set as 10 bar/10 min (Anton-Paar, Monowave 300, Austria). At the end of the reaction, the reaction mixture was cooled and poured into ice water. The precipitated product was filtered, dried, and crystallized from ethanol.

Synthesis of the N-ethylhydrazinecarbothioamide (2)

Isothiocyanatoethane (0.07 mol) was dissolved in absolute ethanol (> 99 %). And this mixture was put in iced bath. As a second mix, hydrazine hydrate (0.21 mol) was dissolved in absolute ethanol (> 99 %). The second mixture was added in first mixture as dropwise. After the dropping process was finished, the reaction continued to be stirred in the ice bath for an additional 1 h. At the end of the reaction the precipitated product was filtered, washed with cooled ethanol, and dried.

Synthesis of the 2-(1-(4-(1H-imidazol-1-yl)phenyl)ethylidene)-N-ethylhydrazine-1-carbothioamide (3)

1-(4-(1*H*-imidazol-1-yl)phenyl)ethan-1-one (0.06 mol) and *N*-ethyl-hydrazinecarbothioamide (0.06 mol) was dissolved in EtOH. The reaction mixture was refluxed for 5 h. At the end of the reaction, the reaction mixture was cooled and precipitated product was filtered, washed with ethanol, and dried.

Synthesis of the target compounds (4a–4l)

2-(1-(4-(1*H*-imidazol-1-yl)phenyl)ethylidene)-*N*-ethylhydrazine-1-carbothioamide and appropriate 2-bromoacetophenone were dissolved in ethanol. The reaction mixture was refluxed to actualize ring closure reaction. At the end of the reaction, the reaction mixture was cooled and poured into ice water. The precipitated product was filtered, dried, and crystallized from hexane.

2-((1-(4-(1H-Imidazol-1-yl)phenyl)ethylidene)hydrazineylidendene)-3-ethyl-4-(p-tolyl)-2,3-dihydrothiazole (4a)

Yield: 79%, M.p.: 272.9-279.9 °C. ^{1}H-NMR (300 MHz, (D_6)DMSO): δ = 1.19 (3H, t, *J* = 7.04, –CH_3), 2.44 (3H, s, –CH_3), 3.84-3.91 (2H, m, –CH_2–), 6.65 (1H, s, thiazole), 7.56 (1H, s, Imidazole), 7.79 (4H, dd, J_1 = 3.89, J_2 = 8.89, *p*-disubstituted benzene), 8.01 (2H, d, *J* = 8.83, *p*-substituted benzene), 8.08 (1H, s, imidazole), 8.34 (2H, d, *J* = 8.86, *p*-substituted benzene), 9.05 (1H, s, imidazole). ^{13}C-NMR (75 MHz, (D_6)DMSO): δ = 13.49 (CH_2CH_3), 14.53 (N=C–CH_3), 21.32 (CH_3), 24.42 (CH_2CH_3), 100.42 (Ar–C), 119.74 (Ar–C), 121.36 (Ar–C), 125.98 (Ar–C), 127.53 (Ar–C), 128.38 (Ar–C), 129.21 (Ar–C), 129.87 (Ar–C), 135.46 (Ar–C), 136.16 (Ar–C), 138.85 (Ar–C), 139.34 (Ar–C), 140.69 (Ar–C), 153.16 (Ar–C), 169.31 (Ar–C). HR-MS (*m/z*): $[M+H]^+$ calc. for $C_{23}H_{23}N_5S$: 402.1747; found: 402.1751.

2-((1-(4-(1H-Imidazol-1-yl)phenyl)ethylidene)hydrazineylidendene)-3-ethyl-4-(4-methoxyphenyl)-2,3-dihydrothiazole (4b)

Yield: 79%, M.p.: 280.8–283.6 °C. ^{1}H-NMR (300 MHz, (D_6)DMSO): δ = 1.16 (3H, t, *J* = 7.01, –CH_3), 2.42 (3H, s, –CH_3), 3.80–3.82 (2H, m, –CH_2–), 3.82 (3H, s, –CH_3), 6.28 (1H, s, thiazole), 7.06 (2H, d, *J* = 8.80, *p*-disubstituted benzene), 7.39 (2H, m, *p*-disubstituted benzene), 7.56 (1H, m, imidazole), 7.78 (2H, m, *p*-disubstituted benzene), 7.98 (2H, m, *p*-disubstituted benzene), 8.08 (1H, m, imidazole), 9.08 (1H, s, imidazole). ^{13}C-NMR (75 MHz, (D_6)DMSO): δ = 12.63 (CH_2CH_3), 15.37 (N=C–CH_3), 54.79 (CH_2CH_3), 56.71 (OCH_3), 98.82 (Ar–C), 101.39 (Ar–C), 113.65 (Ar–C), 115.79 (Ar–C), 118.63 (Ar–C), 120.38 (Ar–C), 121.27 (Ar–C), 122.56 (Ar–C), 123.42 (Ar–C), 124.35 (Ar–C), 126.49 (Ar–C), 128.56 (Ar–C), 129.77 (Ar–C), 131.88 (Ar–C), 136.07 (Ar–C), 136.86 (Ar–C), 139.10 (Ar–C), 153.10 (Ar–C), 163.31 (Ar–C). HR-MS (*m/z*): $[M+H]^+$ calc. for $C_{23}H_{23}N_5OS$: 418.1696; found: 418.1690.

4-(2((1-(4-(1H-Imidazol-1-yl)phenyl)ethylidene)hydrazineylideidene)-3-ethyl-2,3-dihydrothiazol-4-yl)benzonitrile (4c)

Yield: 79%, M.p.: 272.9-279.9 °C. ^{1}H-NMR (300 MHz, (D_6)DMSO): δ = 1.17 (3H, t, *J* = 7.01, –CH_3), 2.45 (3H, s, –CH_3), 3.83–3.87 (2H, m, –CH_2–), 6.59 (1H, s, thiazole),7.72 (2H, d, *J* = 8.44, *p*-disubstituted benzene), 7.83 (2H, m, *p*-disubstituted benzene), 7.85 (1H, s, imidazole), 7.99 (2H, d, *J* = 8.45, *p*-disubstituted benzene), 8.04 (2H, d, *J* = 8.89, *p*-disubstituted benzene), 8.26 (1H, m, imidazole), 9.54 (1H, m, imidazole). ^{13}C-NMR (75 MHz, (D_6)DMSO): δ = 13.81 (CH_2CH_3), 14.32 (N=C–CH_3), 15.50 (CH_2CH_3), 102.15 (Ar–C), 104.73 (Ar–C), 112.24 (Ar–C), 118.88 (Ar–C), 120.99 (Ar–C), 123.11 (Ar–C), 124.15 (Ar–C), 126.51 (Ar–C), 128.91 (Ar–C), 131.05 (Ar–C), 132.20 (Ar–C), 134.38 (Ar–C), 135.68 (Ar–C), 136.51 (Ar–C), 139.69 (Ar–C), 153.75 (Ar–C). HR-MS (*m/z*): $[M+H]^+$ calc. for $C_{23}H_{20}N_6S$: 413.1543; found: 413.1549.

2-((1-(4-(1H-Imidazol-1-yl)phenyl)ethylidene)hydrazineylidendene)-3-ethyl-4-(4-nitrophenyl)-2,3-dihydrothiazole (4d)

Yield: 79%, M.p.: 281.2-284.8 °C. ^{1}H-NMR (300 MHz, (D_6)DMSO): δ = 1.19 (3H, t, *J* = 7.01, –CH_3), 2.44 (3H, s, –CH_3), 3.84-3.92 (2H, m, –CH_2–), 6.65 (1H, s, thiazole), 7.57 (1H, s, imidazole), 7.79 (4H, dd, J_1 = 3.89, J_2 = 8.86, *p*-disubstituted benzene), 8.01 (2H, d, *J* = 8.83, *p*-substituted benzene), 8.08 (1H, s, imidazole), 8.34 (2H, d, *J* = 8.86, *p*-disubstituted benzene), 9.05 (1H, s, imidazole). ^{13}C-NMR (75 MHz, (D_6)DMSO): δ = 12.67 (CH_2CH_3), 13.83 (N=C–CH_3), 15.51 (CH_2CH_3), 102.72 (Ar–C), 105.30 (Ar–C), 120.34 (Ar–C), 122.52 (Ar–C), 123.37 (Ar–C), 125.63 (Ar–C), 126.52 (Ar–C), 126.61 (Ar–C), 128.68 (Ar–C), 129.17 (Ar–C), 131.37 (Ar–C), 136.28 (Ar–C), 136.93 (Ar–C), 138.73 (Ar–C), 148.05 (Ar–C). HR-MS (*m/z*): $[M+H]^+$ calc. for $C_{22}H_{20}N_6O_2S$: 433.1441; found: 433.1457.

2-((1-(4-(1H-Imidazol-1-yl)phenyl)ethylidene)hydrazineylidendene)-3-ethyl-4-(4-fluorophenyl)-2,3-dihydrothiazole (4e)

Yield: 79%, M.p.: 258.7-261.5 °C. ^{1}H-NMR (300 MHz, (D_6)DMSO): δ = 1.15 (3H, t, *J* = 7.04, –CH_3), 2.43 (3H, s, CH_3), 3.78-3.85 (2H, m, –CH_2–), 6.39 (1H, s, thiazole), 7.57 (1H, s, Imidazole), 7.79 (4H, dd, J_1 = 3.89, J_2 = 8.86, *p*-disubstituted benzene), 8.01 (2H, d, *J* = 8.83, *p*-substituted benzene), 8.08 (1H, s, Imidazole), 8.34 (2H, d, *J* = 8.86, *p*-substituted benzene), 9.05 (1H, s, Imidazole). ^{13}C-NMR (75 MHz, (D_6)DMSO): δ = 12.60 (CH_2CH_3), 15.41 (N=C–CH_3), 17.09 (CH_2CH_3), 99.89 (Ar–C), 102.46 (Ar–C), 115.39 (Ar–C), 117.26 (Ar–C), 117.54 (Ar–C), 120.34 (Ar–C), 122.52 (Ar–C), 126.52 (Ar–C), 127.66 (Ar–C), 128.59 (Ar–C), 130.63 (Ar–C), 132.81 (Ar–C), 136.85 (Ar–C), 153.31 (Ar–C), 169.14 (Ar–C). HR-MS (*m/z*): $[M+H]^+$ calc. for $C_{22}H_{20}N_5FS$: 406.1496; found: 406.1504.

2-((1-(4-(1H-Imidazol-1-yl)phenyl)ethylidene)hydrazineylidendene)-4-(4–CHlorophenyl)-3-ethyl-2,3-dihydrothiazole (4f)

Yield: 79%, M.p.: 278.1-280.0 °C. ^{1}H-NMR (300 MHz, (D_6)DMSO): δ = 1.16 (3H, t, *J* = 7.04, –CH_3), 2.43 (3H, s, CH_3), 3.79–3.86 (2H, m, –CH_2–), 6.42 (1H, s, thiazole), 7.50 (1H, d, *J* = 3.39, Imidazole), 7.53 (2H, m, *p*-disubstituted benzene), 7.56 (2H, m, *p*-disubstituted benzene), 7.78 (2H, d, *J* = 8.83, *p*-substituted benzene), 8.00 (2H, d, *J* = 8.83, *p*-substituted benzene), 8.07 (1H, m, Imidazole), 9.05 (1H, s, Imidazole). ^{13}C-NMR (75 MHz, (D_6)DMSO): δ = 12.70 (CH_2CH_3), 15.44 (N=C–CH_3), 45.98 (CH_2CH_3), 100.35 (Ar–C), 102.92 (Ar–C), 120.31 (Ar–C), 122.49 (Ar–C), 126.54 (Ar–C), 128.25 (Ar–C),128.70 (Ar–C), 130.10 (Ar–C), 130.48 (Ar–C), 130.55 (Ar–C), 132.19 (Ar–C), 132.28 (Ar–C), 134.53 (Ar–C), 153.58 (Ar–C), 169.26 (Ar–C). HR-MS (*m/z*): $[M+H]^+$ calc. for $C_{22}H_{20}N_5SCl$: 422.1201; found: 422.1185.

2-((1-(4-(1H-Imidazol-1-yl)phenyl)ethylidene)hydrazineylidendene)-4-(4-bromophenyl)-3-ethyl-2,3-dihydrothiazole (4g)

Yield: 79%, M.p.: 289.5–291.3 °C. ^{1}H-NMR (300 MHz, (D_6)DMSO): δ = 1.16 (3H, t, *J* = 7.01, –CH_3), 2.43 (3H, s, CH_3), 3.79–3.86 (2H, m, –CH_2–), 6.43 (1H, s, thiazole), 7.45 (2H, d, *J* = 8.47, *p*-substituted benzene), 7.56 (1H, m, Imidazole), 7.75 (4H, m, *p*-disubstituted benzene), 8.00 (2H, d, *J* = 8.86, *p*-substituted benzene), 8.07 (1H, m, Imidazole), 9.06 (1H, s, Imidazole). ^{13}C-NMR (75 MHz, (D_6)DMSO): δ = 12.64 (CH_2CH_3), 15.43 (N=C–CH_3), 17.11 (CH_2CH_3), 100.33 (Ar–C), 102.91 (Ar–C), 120.35 (Ar–C), 122.53 (Ar–C), 123.18 (Ar–C), 126.55 (Ar–C), 128.71 (Ar–C), 130.30 (Ar–C), 131.15 (Ar–C), 132.50 (Ar–C), 133.40 (Ar–C), 136.18 (Ar–C), 136.86 (Ar–C), 138.97 (Ar–C), 139.52 (Ar–C), 153.51 (Ar–C), 169.27 (Ar–C). HR-MS (*m/z*): $[M+H]^+$ calc. for $C_{22}H_{20}N_5SBr$: 466.0696; found: 466.0698.

2-((1-(4-(1H-Imidazol-1-yl)phenyl)ethylidene)hydrazineylidendene)-4-([1,1′-biphenyl]-4-yl)-3-ethyl-2,3-dihydrothiazole (4h)

Yield: 79%, M.p.: 259.4–260.7 °C. ^{1}H-NMR (300 MHz, (D_6)DMSO): δ = 1.21 (3H, t, *J* = 6.93, –CH_3), 2.44 (3H, s, CH_3), 3.86–3.93 (2H, m,

–CH_2–), 6.43 (1H, s, thiazole), 7.41 (1H, m, monosubstituted benzene), 7.50 (2H, m, *p*-disubstituted benzene), 7.57 (2H, s, *p*-disubstituted benzene), 7.59 (1H, m, Imidazole), 7.73 (2H, m, monosubstituted benzene), 7.80 (4H, m, *p*-disubstituted benzene), 8.01 (2H, d, $J=8.71$, *p*-substituted benzene), 8.08 (1H, m, Imidazole), 9.07 (1H, s, Imidazole). ^{13}C-NMR (75 MHz, (D_6)DMSO): $\delta=12.69$ (CH_2CH_3), 15.42 (N=C–CH_3), 25.30 (CH_2CH_3), 99.85 (Ar–C), 102.43 (Ar–C), 118.59 (Ar–C), 120.36 (Ar–C), 121.03 (Ar–C), 121.28 (Ar–C), 121.59 (Ar–C), 122.54 (Ar–C), 124.50 (Ar–C), 126.46 (Ar–C), 128.53 (Ar–C), 130.85 (Ar–C), 136.86 (Ar–C), 138.90 (Ar–C), 139.65 (Ar–C), 140.40 (Ar–C), 141.32 (Ar–C), 153.35 (Ar–C), 169.38 (Ar–C). HR-MS (*m/z*): $[M+H]^+$ calc. for $C_{28}H_{25}N_5S$: 464.1903; found: 464.1897.

2-((1-(4-(1H-Imidazol-1-yl)phenyl)ethylidene)hydrazineylidendene)-4-(2,4-dimethylphenyl)-3-ethyl-2,3-dihydrothiazole (4i)

Yield: 80 %, M.p.: 263.3–265.2 °C. ^{1}H-NMR (300 MHz, (D_6)DMSO): $\delta=$ 1.03–1.08 (3H, m, –CH_3), 2.17 (3H, s, –CH_3), 2.34 (3H, s, –CH_3), 2.43 (3H, s, CH_3), 3.42-3.50 (2H, m,–CH_2–), 6.27 (1H, s, thiazole), 7.13 (1H, d, $J=6.78$, 1,2,4-trisubstituted benzene), 7.21 (2H, m, 1,2,4-trisubstituted benzene), 7.85 (2H, d, $J=8.86$, *p*-disubstituted benzene), 7.92 (1H, m, Imidazole), 8.04 (2H, d, $J=8.89$, *p*-substituted benzene), 8.31 (1H, m, Imidazole), 9.69 (1H, s, Imidazole). ^{13}C-NMR (75 MHz, (D_6)DMSO): $\delta=12.46$ (CH_2CH_3), 15.38 (N=C–CH_3), 17.06 (CH_2CH_3), 20.44 (CH_3), 22.12 (CH_3), 99.09 (Ar–C), 101.66 (Ar–C), 121.13 (Ar–C), 122.39 (Ar–C), 123.31 (Ar–C), 126.38 (Ar–C), 128.53 (Ar–C), 129.78 (Ar–C), 131.89 (Ar–C), 136.50 (Ar–C), 137.70 (Ar–C), 139.73 (Ar–C), 140.12 (Ar–C), 152.82 (Ar–C), 169.05 (Ar–C). HR-MS (*m/z*): $[M+H]^+$ calc. for $C_{24}H_{25}N_5S$: 416.1903; found: 416.1891.

2-((1-(4-(1H-Imidazol-1-yl)phenyl)ethylidene)hydrazineylidendene)-4-(2,4-difluorophenyl)-3-ethyl-2,3-dihydrothiazole (4j)

Yield: 72 %, M.p.: 252.8–254.3 °C. ^{1}H-NMR (300 MHz, (D_6)DMSO): $\delta=$ 1.12 (3H, t, $J=7.04$, –CH_3), 2.43 (3H, s, CH_3), 3.67-3.74 (2H, m, –CH_2–), 6.51 (1H, s, thiazole), 7.28 (1H, m, 1,2,4-trisubstituted benzene), 7.48 (1H, m, 1,2,4-trisubstituted benzene), 7.58 (1H, m, Imidazole), 7.60 (1H, m, 1,2,4-trisubstituted benzene), 7.79 (2H, m, *p*-disubstituted benzene), 7.97 (2H, m, *p*-substituted benzene), 8.11 (1H, m, Imidazole), 9.16 (1H, s, Imidazole). ^{13}C-NMR (75 MHz, (D_6)DMSO): $\delta=14.11$ (CH_2CH_3), 15.44 (N=C–CH_3), 25.29 (CH_2CH_3), 101.31 (Ar–C), 101.98 (Ar–C), 104.10 (Ar–C), 104.57 (Ar–C), 114.08 (Ar–C), 119.48 (Ar–C), 120.44 (Ar–C), 122.62 (Ar–C), 124.02 (Ar–C), 126.56 (Ar–C), 128.70 (Ar–C), 129.93 (Ar–C), 132.01 (Ar–C), 132.97 (Ar–C), 133.92 (Ar–C), 135.25 (Ar–C), 136.91 (Ar–C), 162.08 (Ar–C), 168.57 (Ar–C). HR-MS (*m/z*): $[M+H]^+$ calc. for $C_{22}H_{19}N_4F_2S$: 424.1402; found: 424.1407.

2-((1-(4-(1H-Imidazol-1-yl)phenyl)ethylidene)hydrazineylidendene)-4-(2,4-dichlorophenyl)-3-ethyl-2,3-dihydrothiazole (4k)

Yield: 81 %, M.p.: 249.8–251.2 °C. ^{1}H-NMR (300 MHz, (D_6)DMSO): $\delta=$ 1.10 (3H, t, $J=7.02$, –CH_3), 2.43 (3H, s, CH_3), 3.43–3.61 (2H, m, –CH_2–), 6.48 (1H, s, thiazole), 7.58 (1H, m, Imidazole), 7.62 (1H, m, 1,2,4-trisubstituted benzene), 7.66 (1H, m, 1,2,4-trisubstituted benzene), 7.80 (2H, m, *p*-disubstituted benzene), 7.85 (1H, m, 1,2,4-trisubstituted benzene), 7.99 (2H, dd, $J_1=8.87$, $J_2=17.13$, *p*-substituted benzene), 8.11 (1H, m, Imidazole), 9.22 (1H, s, Imidazole). ^{13}C-NMR (75 MHz, (D_6)DMSO): $\delta=12.75$ (CH_2CH_3), 15.44 (N=C–CH_3), 25.28 (CH_2CH_3), 101.49 (Ar–C), 104.09 (Ar–C), 119.61 (Ar–C), 120.59 (Ar–C), 121.79 (Ar–C), 122.78 (Ar–C), 123.50 (Ar–C), 126.46 (Ar–C), 127.22 (Ar–C), 128.69 (Ar–C), 129.84 (Ar–C), 130.96 (Ar–C), 132.01 (Ar–C), 133.24 (Ar–C), 133.89 (Ar–C), 135.47 (Ar–C), 136.82 (Ar–C), 139.20 (Ar–C), 168.46 (Ar–C). HR-MS (*m/z*): $[M+H]^+$ calc. for $C_{22}H_{19}N_5SCl$: 458.0811; found: 456.0819.

2-((1-(4-(1H-Imidazol-1-yl)phenyl)ethylidene)hydrazineylidendene)-4-(3,4-dichlorophenyl)-3-ethyl-2,3-dihydrothiazole (4 l)

Yield: 71 %, M.p.: 259.2–261.7 °C. ^{1}H-NMR (300 MHz, (D_6)DMSO): $\delta=$ 1.16 (3H, t, $J=7.05$, –CH_3), 2.43 (3H, s, CH_3), 3.79-3.86 (2H, m, –CH_2–), 6.42 (1H, s, thiazole), 7.50 (1H, m, Imidazole), 7.54 (2H, m, 1,2,4-trisubstituted benzene), 7.56 (1H, m, 1,2,4-trisubstituted benzene), 7.77 (2H, m, *p*-disubstituted benzene), 8.00 (2H, d, $J=$ 8.83, *p*-substituted benzene), 8.07 (1H, m, Imidazole), 9.05 (1H, s, Imidazole). ^{13}C-NMR (75 MHz, (D_6)DMSO): $\delta=13.49$ (CH_2CH_3), 14.63 (N=C–CH_3), 41.39 (CH_2CH_3), 102.81 (Ar–C), 121.08 (Ar–C), 121.90 (Ar–C), 122.23 (Ar–C), 127.59 (Ar–C), 129.52 (Ar–C), 131.23 (Ar–C), 131.47 (Ar–C), 131.67 (Ar–C), 132.09 (Ar–C), 132.60 (Ar–C), 135.05 (Ar–C), 135.25 (Ar–C), 138.16 (Ar–C), 139.95 (Ar–C), 153.45 (Ar–C), 169.38 (Ar–C). HR-MS (*m/z*): $[M+H]^+$ calc. for $C_{22}H_{19}N_5SCl$: 456.0811; found: 456.0823.

Cytotoxicity Tests

The MTT test is a cytotoxicity assay that is used to identify living cells by the color change of the formed formazan salt.[32] Cytotoxicity tests were performed using HepG2, MCF-7 and NIH3T3 cell lines in accordance with the MTT procedure previously specified by our team.[33–35]

Antifungal Studies

Determination of the minimum inhibitory concentration (MIC)

The antifungal activity of the synthesized compounds was examined using 96-well microtiter plates and the broth microdilution method from Clinical and Laboratory Standards Institute (CLSI) document M27-A3. Briefly, the inoculum size was adjusted to 0.5–2.5×10^3 Candida cells/mL using RPMI1640 media (pH:7.0) supplemented with 2% glucose. The microplates were incubated at 37 °C for 24—48 h. The first well with total growth inhibition was referred to as the minimum inhibitory concentration (MIC).[36]

Effects on mature biofilm formation

Antibiofilm activity of the synthesized compounds were tested. To form mature biofilm formation, sterile 96-well flat-bottomed microplate was seeded with standard inoculum (0.5 McFarland) of Candida reference strains (100 µL each well), followed by incubation for 24 h at 37 °C. After the incubation, unattached cells were removed by washing the microplates three times in phosphate-buffered saline (PBS). Based on their capacity to produce biofilms, synthesized compounds were tested at sub-inhibitory concentrations of $^1/_2\times$MIC, MIC, and 2×MIC. The compounds were added to each well and incubated for 24 h at 37 °C. Incubated overnight, the microplates were washed three times with PBS and 100 µ of 0.1% crystal violet was added to each well. The microplates were washed three times with PBS after 5 min at room temperature. Then, 150 µL of 0.04 N HCl-isopropanol and 50 µL of 0.25% sodium dodecyl sulfate (SDS) were added to each well. A microplate reader was used to read the absorbance values at 590 nm. Untreated biofilm served as the growth control. The values of the experimental group and growth control were used to determine the percentage of inhibition. Biofilm inhibition rate = $(OD_{control}-OD_{sample}/OD_{control})\times 100$.[37]

Molecular docking

Molecular docking studies were performed using an *in-silico* procedure to define the binding modes of active compound in the active regions of VEGFR-2. X-ray crystal structures of the VEGFR-2 (PDB ID: 4ASE)[38] were retrieved from the Protein Data Bank server (www.pdb.org, accessed 01 May 2023). The docking procedure was performed using Schrödinger Maestro[39] interface, LigPrep module[40] and Glide module,[41] and docking runs were conducted in standard precision (SP) docking mode.

Molecular dynamic simulations

Molecular dynamic (MD) simulations are considered an important computational tool for evaluating the time-dependent stability of a ligand in an active site for a drug-receptor complex.[42] MD simulations for 40 ns were carried out to ensure the stability of the identified hits from the docking result. We performed the Desmond application[43] using the standard force field (OPLS3e) of the Schrodinger Suite with a transferable intermolecular potential with a 3 points (TIP3P) water model followed by energy minimization of the complex.[44] The neutralization of the system was achieved using Na^+ and Cl^- ions. The MD simulation was performed following the completion of the system setup. Rg (radius of gyration), root mean square fluctuation (RMSF) and root mean square deviation (RMSD) values were calculated by the Desmond application.[45]

Author Contributions

D.O. conceived and designed the experiments; D.O. and B.K. performed the synthesis; N.B.B. and G.B.Y. performed the antifungal activity tests; D.O. and Y.O. performed the anticancer activity tests; D.O. performed the molecular docking and molecular dynamic studies; B.K. and Z.A.K. performed analysis studies; D.O. and B.K. wrote the article. Y.O. and ZAK edited the article.

Acknowledgements

As the authors of this study, we thank Anadolu University Faculty of Pharmacy Central Analysis Laboratory for their support and contributions.

Conflict of Interests

The authors declare no conflict of interest.

Data Availability Statement

The data that support the findings of this study are available in the supplementary material of this article.

Keywords: imidazole · 2,3-dihydrothiazole · VEGFR-2 · molecular docking · molecular dynamics

[1] A. M. Srour, D. H. Dawood, E. S. Nossier, R. A. El-Shiekh, A. E. Mahmoud, A. G. Hussien, M. M. Omran, M. M. Ali, *J. Mol. Struct.* **2023**, *1271*, e134130.
[2] https://www.who.int (Accessed Date:05. 04. 2023).
[3] I. H. Ali, H. T. Abdel-Mohsen, M. M. Mounier, M. T. Abo-elfadl, A. M. El Kerdawy, I. A. Y. Ghannam, *Bioorg. Chem.* **2022**, *126*, e105883.
[4] M. Zengin, O. Unsal Tan, R. K. Arafa, A. Balkan, *Bioorg. Chem.* **2022**, *121*, e105696.
[5] M. A. Mahmoud, A. F. Mohammed, O. I. A. Salem, S. M. Rabea, B. G. M. Youssif, *J. Mol. Struct.* **2023**, *1282*, e135165.
[6] M. M. Alanazi, H. Elkady, N. A. Alsaif, A. J. Obaidullah, W. A. Alanazi, A. M. Al-Hossaini, M. A. Alharbi, I. H. Eissa, M. A. Dahab, *J. Mol. Struct.* **2022**, *1253*, e132220.
[7] X. R. Wang, S. Wang, H. X. Mu, K. Y. Xu, X. T. Wang, J. T. Shi, Q. H. Cui, L. W. Zhang, S. W. Chen, *Eur. J. Med. Chem.* **2022**, *244*, e114821.
[8] A. Hamdi, H. W. El-Shafey, D. I. A. Othman, A. S. El-Azab, N. A. AlSaif, A. A. M. Abdel-Aziz, *Bioorg. Chem.* **2022**, *122*, e105710.
[9] A. M. El-Naggar, A. M. A. Hassan, E. B. Elkaeed, M. S. Alesawy, A. A. Al-Karmalawy, *Bioorg. Chem.* **2022**, *123*, e105770.
[10] S. D. Hadiyal, J. N. Lalpara, B. B. Dhaduk, H. S. Joshi, *Mol. Diversity* **2023**, *27*, e1345.
[11] F. O. Ashmawy, S. M. Gomha, M. A. Abdallah, M. E. A. Zaki, S. A. Al-Hussain, M. A. El-Desouky, *Molecules.* **2023**, *28*, e4270.
[12] A. K. El-Damasy, H. Jin, M. A. Sabry, H. J. Kim, M. M. Alanazi, S. H. Seo, E. K. Bang, G. Keum, *Medicina.* **2023**, *59*, e1076.
[13] J. Jadeja, M. Savant, *J. Iran. Chem. Soc.* **2023**, *20*, e1491.
[14] R. Aggarwal, M. Hooda, P. Kumar, S. Kumar, S. Singh, R. Chandra, *Bioorg. Chem.* **2023**, *136*, e106524.
[15] G. R. S. Ashour, A. F. Qarah, A. F. Alrefaei, A. I. Alalawy, A. Alsoliemy, A. M. Alqahtani, et al., *J. Saudi Chem. Soc.* **2023**, *27*, e101669.
[16] Y. Nandurkar, M. R. Bhoye, D. Maliwal, R. R. S. Pissurlenkar, A. Chavan, S. Katade, P. C. Mhaske, *Eur. J. Med. Chem.* **2023**, *258*, e115548.
[17] M. E. Salem, E. M. Mahrous, E. A. Ragab, M. S. Nafie, K. M. Dawood, *BMC. Chem.* **2023**, *17*, e51.
[18] M. A. Assiri, T. E. Ali, M. N. Alqahtani, Ali A. Shati, Mohammed Y. Alfaifi, Serag E. I. Elbehairi, *Synth. Commun.* **2023**, *53*, e1240.
[19] R. I. Al-Wabli, A. R. Al-Ghamdi, I. P. Primsa, H. A. Ghabbour, M. H. Al-Agamy, I. H. Joe, M. I. Attia, *J. Mol. Struct.* **2018**, *1166*, e121.
[20] F. Zani, P. Mazzal, S. Benvenutiz, F. Severi, L. Malmusiz, G. Vampa, L. Antolini, *Eur. J. Med. Chem.* **1995**, *30*, e729.
[21] A. Macchiarulo, G. Costantino, D. Fringuelli, A. Vecchiarelli, F. Schiaffella, R. Fringuelli, *Bioorg. Med. Chem.* **2022**, *11*, e3415.
[22] D. Zampieri, M. G. Mamolo, E. Laurini, G. Scialino, E. Banfi, L. Vio, *Bioorg. Med. Chem.* **2008**, *16*, e4516.
[23] M. Y. Wani, A. Ahmad, R. A. Shiekh, K. J. Al-Ghamdi, A. J. F. N. Sobral, *Bioorg. Med. Chem.* **2015**, *23*, e4172.
[24] S. Poyraz, H. A. Döndaş, J. M. Sansano, S. Belveren, C. Yamali, M. Ülger, N. Y. Döndaş, B. N. Sağlık, C. M. Pask, *J. Mol. Struct.* **2023**, *1273*, e134303.
[25] L. R. Peixoto, P. L. Rosalen, G. L. S. Ferreira, I. A. Freires, F. G. de Carvalho, L. R. Castellano, R. D. Castro, *Arch. Oral Biol.* **2017**, *73*, e179.
[26] https://bpsbioscience.com/vegfr2-kdr-kinase-assay-kit-40325.
[27] K. Sargsyan, C. Grauffel, C. Lim, *J. Chem. Theory Comput.* **2017**, *13*, e1518.
[28] D. Osmaniye, Ş. Karaca, B. Kurban, M. Baysal, I. Ahmad, H. Patel, Y. Ozkay, Z. A. Kaplancıklı, *Bioorg. Chem.* **2022**, *122*, e105709.
[29] I. Ahmad, D. Kumar, H. Patel, *J. Biomol. Struct. Dyn.* **2022**, *40*, e7991.
[30] R. Zrieq, I. Ahmad, M. Snoussi, E. Noumi, M. Iriti, F. D. Algahtani, H. Patel, M. Saeed, M. Tasleem, S. Sulaiman, K. Aouadi, A. Kadri, *Int. J. Mol. Sci.* **2021**, *22*, e10693.
[31] A. Khezri, A. Karimi, F. Yazdian, M. Jokar, S. R. Mofradnia, H. Rashedi, Z. Tavakoli, *Int. J. Biol. Macromol.* **2018**, *114*, e972.
[32] M. V. Berridge, P. M. Herst, A. S. Tan, *Biotechnol. Annu. Rev.* **2005**, *11*, e127.
[33] D. Osmaniye, B. N. Sağlık, N. Khalilova, S. Levent, G. Bayazıt, Ü. D. Gül, Y. Ozkay, Z. A. Kaplancıklı, *ACS Omega* **2023**, *8*, e6669.
[34] D. Osmaniye, B. Korkut Çelikateş, B. N. Sağlık, S. Levent, U. Acar Çevik, B. Kaya Çavuşoğlu, S. Ilgın, Y. Ozkay, Z. A. Kaplancıklı, *Eur. J. Med. Chem.* **2021**, *210*, e112979.
[35] D. Osmaniye, S. Levent, C. M. Ardıç, Ö. Atlı, Y. Özkay, Z. A. Kaplancıklı, *Phosphorus Sulfur Silicon Relat. Elem.* **2018**, *193*, e249.
[36] M. Aydin, A. Ozturk, T. Duran, U. O. Ozmen, E. Sumlu, E. B. Ayan, E. N. Korucu, *J. Med. Mycol.* **2023**, *33*, e101327.
[37] A. Ozturk, O. Abdulmajed, M. Aydin, *Ann. Med. Res.* **2020**, *27*, e2041.
[38] M. McTigue, B. W. Murray, J. H. Chen, Y. L. Deng, J. Solowiej, R. S. Kania, *Proc. Natl. Acad. Sci. USA* **2012**, *109*, e18281.

[39] Maestro, 10.6, Schrödinger, LLC: New York, NY, USA, **2020**.
[40] Schrödinger, LigPrep, version 3.8, Schrödinger, LLC, New York, NY, USA, **2020**.
[41] Schrödinger, Glide, version 7.1, Schrödinger, LLC: New York, NY, USA, **2020**.
[42] X. Liu, D. Shi, S. Zhou, H. Liu, H. Liu, X. Yao, *Expert Opin. Drug Discovery* **2018**, *13*, e23.
[43] M.-D. I. Tools, Schrödinger, LLC, New York, NY, 2020, Schrödinger Release 2018–3: Prime, **2018**.
[44] A. Saral, P. Sudha, S. Muthu, S. Sevvanthi, P. Sangeetha, S. Selvakumari, *Heliyon* **2021**, *7*, e07529.
[45] S. Release, 1: Desmond molecular dynamics system, version 3.7, DE Shaw Research, New York, NY, Maestro-Desmond Interoperability Tools, version, 3, **2014**.

Manuscript received: June 27, 2023
Accepted manuscript online: July 28, 2023
Version of record online: August 21, 2023